Journal of Molecular Liquids 276 (2019) 120–133

Contents lists available at ScienceDirect

Journal of Molecular Liquids

journal homepage: www.elsevier.com/locate/molliq

Two new 8-hydroxyquinoline derivatives as an efficient corrosion inhibitors for mild steel in hydrochloric acid: Synthesis, electrochemical, surface morphological, UV–visible and theoretical studies

M. Rbaa [a], F. Benhiba [b], I.B. Obot [c], H. Oudda [b], I. Warad [d], B. Lakhrissi [a], A. Zarrouk [e,*]

[a] Laboratory Agro-Resources, Polymers and Process Engineering, Department of Chemistry, Faculty of Sciences, Ibn Tofail University, PO Box 133, 14000 Kenitra, Morocco
[b] Laboratory of separation processes, Faculty of Science, University Ibn Tofail, PO Box 133, 14000 Kenitra, Morocco
[c] Centre of Research Excellence in Corrosion, King Fahd University of Petroleum and Minerals, Dhahran, Saudi Arabia
[d] Department of Chemistry, AN-Najah National University, P.O. Box 7, Nablus, Palestine
[e] Laboratory of Materials, Nanotechnology and Environment, Mohammed V University, Faculty of Science, 4Av. ibn Battuta, B.P. 1014 Rabat, Morocco

ARTICLE INFO

Article history:
Received 29 May 2018
Received in revised form 10 November 2018
Accepted 21 November 2018
Available online 29 November 2018

Keywords:
Synthesis
Quinoline derivatives
Mild steel
Electrochemical techniques
UV–Visible spectrophotometry
Theoretical studies

ABSTRACT

The novel heterocyclic compounds, mainly based on the 8-hydroxyquinoline moiety, namely (8-hydroxyquinolin-5-yl) methyl-4-chlorobenzoate Q1 and (8-hydroxyquinolin-5-yl) methyl-4-nitrobenzoate Q2 have been synthesized and identified through different spectroscopic methods (FTIR, ^{1}H, ^{13}C NMR, and Elemental analysis (*EA*)). Q_1 and Q_2 were estimated as corrosion inhibitors of mild steel (*MS*) in the aggressive environment (1 M HCl) utilizing a weight technique (weight loss measurements) and the non-weight techniques (electrochemical techniques), Density Functional Theory (*DFT*) and Monte Carlo Simulations (*MC*). However, to better gather information on bonding mechanism of MS surface/inhibitors/1 M HCl medium, the corrosion protection was once also investigated with the aid of ultraviolet-visible spectrophotometry (UV–Vis). Surface studies (SEM) revealed that the HCl medium protected by Q_1 and Q_2 could prevent the surface damage and decrease the roughness. The results clearly exhibit that the inhibition performance (η %) will increase with an increase in the concentration of Q_1 and Q_2 achieves maximum value of 96% (Q_1) and 92% (Q_1) at optimal concentration (10^{-3} M). Withal, potentiodynamic polarization test results exhibited the influence of Q_1 and Q_2 on both anodic and cathodic reactions suppression. Inhibitors formed protective layers on metal surface through adsorption as per Langmuir model. The metal dissolution and inhibitor adsorption phenomena have been studied through the estimation of thermodynamic parameters. *DFT* calculations and *MC* simulations were exploited to describe the electronic and adsorption properties of Q_1 and Q_2. The records of both techniques supported the experimental findings.

1. Introduction

Metal corrosion is an unavoidable difficulty for industries. Mild steel is the most extensively employed metal in industrial applications because of its excellent mechanical characteristics and inexpensiveness, [1]. A Large quantity of the mild steel, as well as other iron alloys, is destroyed by corrosion in aggressive media, especially in acid environments which cost billions of dollars every year [2]. This situation has grown to be a more important task for corrosion engineers and the scientific neighborhood. From an economic point of view, stopping or slowing down this deterioration has become obligatory. The only solution to this undesirable problem is to use corrosion safety methods. Corrosion inhibitors are commonly added to the aggressive acids to prevent the severe metal dissolution during acid treatment [3]. Therefore, specific amounts of various synthetic corrosion inhibitors are added to the HCl solution for mild steel corrosion control. Recently, 8-hydroxyquinoline derivatives compounds have gained significant attention in corrosion science [4,5]. Literature reviews reveal that heterocycles compounds based on 8-hydroxyquinolines are used as efficient corrosion inhibitors for metals in an acid medium [6,7].

The novelty of this work is synthesis of two new compounds based on 8-hydroxyquinoline, to obtain a new variety of multifunctional heterocycles based on the 8-hydroxyquinoline moiety, to create several reactive sites in order to apply as steel corrosion inhibitors in an acid medium. In addition, the synthesized compounds were identified by Infrared (*IR*), nuclear magnetic resonance (NMR ^{1}H, ^{13}C) and elementary analysis (*EA*). The corrosion inhibiting action find out about of these compounds was evaluated by electrochemical methods (potentiodynamic polarization, impedance spectroscopy) and gravimetric methods

* Corresponding author.
E-mail address: azarrouk@gmail.com (A. Zarrouk).

https://doi.org/10.1016/j.molliq.2018.11.104
0167-7322/

(mass loss).in addition, *MC* simulations and *DFT* calculations are employed to discuss the adsorption configuration to give an explanation for the corrosion inhibition mechanism of utilized inhibitors on the MS surface. The corrosion inhibition performance of the compound Q_1 is significant compared with that of the compound Q_2 and this is explained by the existence of a mesomeric electron donor group (—Cl) carried by Q_1 improving thus its adsorption capacity on the metal [8,9].

2. Experimental details

2.1. General information

For the synthesis of these new products, the mark of reagents, techniques and melting points were utilized and made as a work that we published previously [10].

The steel rooms were weighed and then submerged in HCl solutions without and with the compounds for 6 h. After, the specimens were withdrawn and cleaned by acetone, and then dried and weighed. The chemical composition of the used mild steel is (wt%): C, 0.11; Si, 0.24; Mn, 0.47; Cr, 0.12; Mo, 0.02; Ni, 0.1; Al, 0.03; Cu, 0.14; Co, <0.012; V, <0.003; W, 0.06; Fe, balance.

2.2. Organic synthesis

2.2.1. General procedure for the preparation of the compounds Q_1 and Q_2

A solution of 5-hydroxymethylquinolin-8-ol (10 mmol), 4-alkylbenzoic acid (10 mmol) in absolute THF (50 mL), and a solution of concentrated HCl (37%) was refluxed under stirring for 10 h.

The use of hexane-acetone (6:4, v/v) as the mobile phase and thin layer chromatography is to follow the reaction. After completion, the reaction mixture was cooled to room temperature, diluted with water (20 mL), and extracted with dichloromethane (3 × 20 mL). The combined organic layers were dried over anhydrous $MgSO_4$, filtered and the solvent was removed by rotary evaporation under vacuum. The obtained crude residue was washed with acetone and purified by chromatography on a silica gel column utilizing dichloromethane/hexane (85:15, v/v), and then recrystallized from absolute ethanol (Scheme 1).

The structure, names, abbreviations, yields, and physicochemical characteristics of the synthesized compounds are shown in Tables 1 and 2.

Compound 5-hydroxymethylquinolin-8-ol (HMHQ) was synthesized by adopting the method already described in the literature [11].

2.3. Weight loss measurements

Mass loss measurements were made in accordance with an experimental protocol already mentioned in a preceding work [12]. The corrosion rate is appreciated through the relationship (Eq. (1)).

$$W_{corr} = \frac{m_i - m_f}{S \times t} \tag{1}$$

where initial weight symbolized by m_i, final weight symbolized by m_f, immersion time symbolized by t and the surface of panel symbolized by S.

The inhibition performance $\eta_W(\%)$ is appreciated as follows (Eq. (2)):

$$\eta_W(\%) = \left(\frac{W^0_{corr} - W_{corr}}{W^0_{corr}}\right) \times 100 \tag{2}$$

where $W_{corr'}$ and W_{corr} according to the abbreviations chosen are the corrosion rates in the absence and the presence of Q_1 and Q_2, respectively.

2.4. Electrochemical tests

As the method of mass loss, the electrochemical techniques have been described in the same previous public work [13]. The values of performance $\eta_{PDP}(\%)$ are calculated utilizing Eq. (3).

$$\eta_{PDP}(\%) = \left(\frac{i_{corr} - i'_{corr}}{i_{corr}}\right) \times 100 \tag{3}$$

where i_{corr} is the corrosion current density in the absence of Q_1 and Q_2, and $i_{corr'}$ is the corrosion current density with Q_1 and Q_2 [13].

The conventional electrochemical impedance spectroscopy (*SIE*) were run at a frequency ranging from 100 kHz up to 100 mHz with a. c. amplitude 10 mV at OCP [13]. All the electrochemical experiments were performed at room temperature (298 K) but potentiodynamic polarization study was carried out at various temperature ranges from 298 to 328 K for calculating kinetic and thermodynamic parameters. Nyquist plots were made from these experiments. The best fit of the experiments was done utilizing ZView 2 software. Eq. (4) was utilized to estimate the η_{EIS} (%):

$$\eta_{EIS}(\%) = \left(\frac{R_p R'_p}{R_p}\right) \times 100 \tag{4}$$

where R_p is of polarization resistance in presence of Q_1 and Q_2, and R'_p is the polarization value without Q_1 and Q_2.

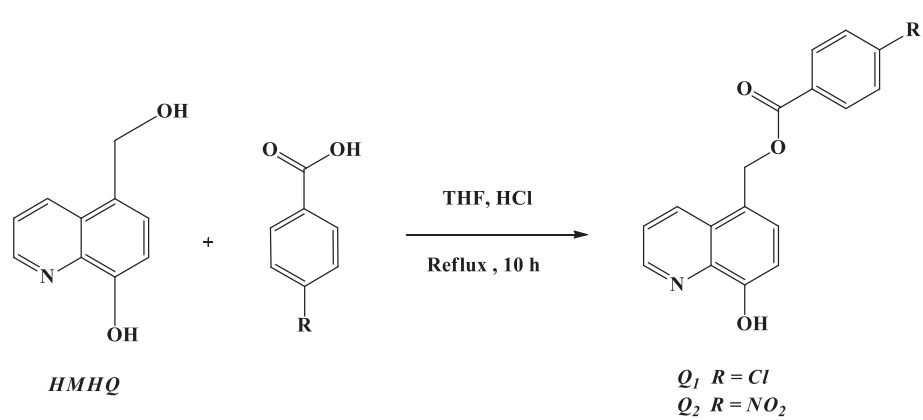

Scheme 1. Synthetic route for the preparation of the compounds Q_1 and Q_2.

Table 1
Molecular structure of Q_1 and Q_2.

Product abbreviation	Chemical structure	Compound name	Molecular weight: (g/mol)
Q_1	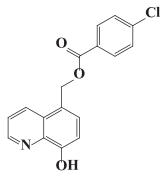	(8-Hydroxyquinolin-5-yl) methyl 4-chlorobenzoate	313,74
Q_2	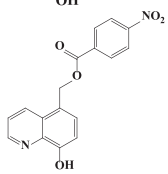	(8-Hydroxyquinolin-5-yl) methyl 4-nitrobenzoate	324,29

2.5. Surface analysis

2.5.1. Scanning electron microscopy (SEM)

After immersing in a solution of HCl (1 M) for 6 h except and with optimum concentration (1 mM) of quinoline derivatives, the surface of the steel was analyzed by way of scanning electron microscopy (*SEM*). The method of sample preparation in our steel was identical to that described in Section 2.3. The *SEM* images was performed on the surface of the MS panels in the absence and in the presence of Q_1 and Q_2 to analyze the morphology of the deposited protective layers.

2.5.2. UV–Visible spectra

To discover more data on the bonding mechanism of *MS* surfaces/compounds/aggressive environment, corrosion protection was also investigated by means of ultraviolet-visible spectrophotometry (UV–Vis), before and after immersion of the *MS* sample for 48 h. The Jenway ultraviolet-visible spectrophotometer (series 67) was once utilized for this analysis.

2.5. Theoretical studies

2.5.3. Density functional theory (DFT) study

To apprehend the mechanism between the molecular properties of Q_1 and Q_2 and their inhibition performance, theoretical calculations utilizing DFT are effectuated out.

Calculation of quantum parameters and optimization of Q_1 and Q_2 molecular geometry was carried out by means of DFT the usage of the 6-31G base set (*d*, *p*). The electronic correlation was blanketed via adopting the Becke$_3$-Lee-Yang-Parr (B_3LYP) procedures. The Gaussian program 09 W was utilized to calculate these quantum parameters.

2.5.4. Monte Carlo simulations

MC simulations utilizing simulated annealing method had been carried out to quantify the adsorption of Q_1 and Q_2 on Fe (110) surface. The simulation box consisted of 5 floors of iron atoms split along the (110) plane. A supercell of (10 × 10) was created and vacuum layer of 50 nm height was fabricated. Optimized Q_1 and Q_2 molecules were placed near the surface of the Fe plane (110) adopt the simulated annealing adsorption detection module with the "COMPASS" force field. The simulations were performed under fine convergence conditions, while every simulation went via 5 cycles at 50,000 steps per cycle. Lowest adsorption energies were obtained and documented for Q_1 and Q_2 as they interact with the iron surface.

3. Results and discussion

3.1. Gravimetric measurements

The weight loss approach was utilized to study the impact of the concentration of the two compounds Q_1 and Q_2 on the corrosion inhibition of *MS* in 1 M HCl. The inhibitory performance "η_w %", and other parameters of this approach have been described in Table 3. Conscientious examination of the results showed that the inhibition performance will increase with increasing of Q_1 and Q_2 synthesized molecules concentration. Maximum values of (inhibition performance) 95.2% for Q_1 and 92.4% for Q_2 had been acquired at optimum concentration. It has been said that at decrease concentrations when the concentration increases the inhibitors are ideally adsorbed via flat orientation, surface coverage and thereby inhibition performance increases. Therefore, after the optimum awareness of Q_1 and Q_2, the inhibition overall performance does not exchange significantly.

The excessive inhibition performance of Q_1 significant to Q_2 is explained to the existence of electron donating —Cl group in Q_1 so enhances its ability to donate charges to the metal in the course of the adsorption progress.

3.2. Potentiodynamic polarization curves

The inhibition mechanism of Q_1 and Q_2 on *MS* corrosion in 1 M HCl solution was also studied through Tafel curves. Results given in Fig. 1 clearly depict that both anodic and cathodic branches shifted to lower current densities, indicating the mixed type inhibition effects of the inhibitors. The potentiodynamic polarization parameters were listed in Table 4, these are i_{corr}, corrosion potential (E_{corr}), cathodic Tafel slope (β_c) and anodic Tafel slope (β_a). From Table 4, slight displacement

Table 2
Yields and physicochemical characteristics of the compounds Q_1 and Q_2.

Compounds	M_p (°C)	Spectral data	Solubility (mg/ml)
Q_1	170	**^{1}H:** δ_{ppm} = 5.05 (s, 1H, OH), 4.19 (S, 2H, CH_2), 7.07–8.86 (m, 9H, ArH). **^{13}C:** δ_{ppm} = 49.38 (CH_2), 153.90 (Ar C—OH), 167.26 (C=O), 139.32(C—Cl), 131.82–128.34 (ArCH-benzene ring), 129.50 (ArC-benzene ring), 110.85–122.56–123.36–148.48 (ArCH-quinoline), 127.35–132.46–142.14 (ArC-quinoline). **Elemental analysis:** - Calculated: C, 65.08%; H, 3.86%; N, 4.46%. - Obtained: C, 65.02%; H, 3.70%; N, 4.70%.	1 mg/ml in DMSO 1 mg/ml in DMF 1 mg/2 ml in $CHCl_3$ *Insoluble in hexane*
Q_2	165	**^{1}H**: δ_{ppm} = 4.39 (s, 1H, OH), 4.35 (S, 2H, CH_2), 7.05–8.61 (m, 9H, ArH). **^{13}C:** δ_{ppm} = 59.84 (CH_2), 146.04 (Ar C—OH), 152.26 (C=O), 146.48(C-NO_2), 123.66–128.54 (ArCH-benzene ring), 136.2 (ArC-benzene ring), 114.59–119.90–125.92–134.17–145.07 (ArCH-quinoline), 127.84–128.75–139.98 (ArC-quinoline). **Elemental analysis:** - Calculated: C, 62.96%; H, 3.73%; N, 9.64%. - Obtained: C, 62.87%; H, 3.77%; N, 9.66%.	*1 mg/ml in DMSO* *1 mg/ml in DMF* *1 mg/3 ml in $CHCl_3$* *Insoluble in hexane*

Table 3
Corrosion rate and inhibitory efficicacy obtained by gravimetry at different concentrations of the test compounds (Q_1 and Q_2).

Medium	Conc. (M)	W_{corr} (mg cm^{-2} h^{-1})	θ	η_w(%)
Blank	0	25.00	–	–
Q_1	10^{-6}	4.20	0.832	83.20
	10^{-5}	3.23	0.870	87.08
	10^{-4}	2.23	0.910	91.08
	10^{-3}	1.20	0.952	95.20
Q_2	10^{-6}	5.66	0.773	77.36
	10^{-5}	4.70	0.812	81.20
	10^{-4}	3.45	0.862	86.20
	10^{-3}	1.90	0.924	92.40

Table 4
Electrochemical parameters of polarization of MS corrosion in 1 M HCl without and with addition of Q_1 and Q_2 compounds at different concentrations at 298 K.

Medium	[C] (M)	$-E_{corr}$ (mV vs. SCE)	i_{corr} (μA cm^{-2})	Tafel slopes (mV dec^{-1})		θ	η_{PDP} (%)
				$-\beta_c$	β_a		
Blank	0	506.0	983.00	92.0	150.0	–	–
Q_1	10^{-3}	508.6	50.41	146.4	45.8	0.948	94.8
	10^{-4}	501.0	59.15	123.2	19.6	0.939	93.9
	10^{-5}	503.9	61.56	111.9	100.4	0.937	93.7
	10^{-6}	511.7	292.89	103.0	72.9	0.702	70.2
Q_2	10^{-3}	508.7	75.85	121.6	175.0	0.922	92.2
	10^{-4}	508.3	147.75	179.5	128.3	0.850	85.0
	10^{-5}	501.4	156.26	224.3	131.6	0.941	84.1
	10^{-6}	510.82	196.62	235.6	141.2	0.800	80.0

was observed in the shift of the E_{corr} values, in the presence of various concentrations of compounds Q_1 and Q_2 in 1 M HCl, this maximum displacement was 5.7 mV/*SCE*. These observations indicate that the examined compounds act in each cathodic and anodic domain, so these compounds are mixed type inhibitors [14].

Addition of Q_1 and Q_2 to the corrosive environment causes a modification of cathodic Tafel slope (β_c), indicating that the Q_1 and Q_2 have a direct influence on the kinetics of hydrogen evolution. Also, when compared corrosive environment, the values of the (β_a) changed irregularly in the presence of Q_1 and Q_2, which indicates that the anodic reaction is affected by the presence of Q_1 and Q_2 [15].

η_p (%) values are higher in comparison to those obtained utilizing the gravimetric method. Such difference could be due to the fact that immersion times are different for the two methods. However, the potentiodynamic polarization measurements give the same order of inhibition efficiencies of the two compounds as deduced from weight loss measurements.

3.3. Electrochemical impedance spectroscopy (EIS)

Another important electrochemical technique, *EIS* is a non-destructive technique to evaluate the inhibition performance of corrosion from the interaction between metal and corrosion in HCl as aggressive media. The main index expressing the corrosion inhibition performance is the corrosion resistance which is currently measured as the area enclosed by the loop in Nyquist plot. For a good understanding of the corrosion phenomenon, the mechanism of electrochemical processes, especially the corrosion aspects taking place between the metal surface and electrolyte was comprehensively considered. The corrosion behavior of *MS* immersed in 1 M HCl solution in the presence and absence of different concentrations of Q_1 and Q_2 was investigated utilizing *EIS* over a frequency range of 100 kHz to 100 mHz after immersion in solutions for 30 min. The impedance data was fitted with an appropriate electrical equivalent circuit (Fig. 4). Nyquist and Bode plots of the samples of *MS* in 1 M HCl solutions are depicted in Figs. 2 and 3. According to these figures all plots show only one time constant and the semicircular shape did not change after addition of inhibitors [16,17]. This means that the corrosion reaction is under charge transfer control and the corrosion mechanism did not change. It can be seen from the Nyquist plots that the increase in inhibitor concentration resulted in the increase of diameter of Nyquist plots. This can imply the fact that the organic molecules adsorbed on the active sites of metal surface. A one-time constant electrical equivalent circuit ($R(RQ)$) was employed for modeling of impedance plots. In the model utilized the R_s, R_p and *CPE* are the solution resistance, polarization resistance and constant phase element of double layer, respectively.

It can be seen from Figs. 2–4 and Table 5 that by the increase of Q_1 and Q_2 concentration the values of low frequency impedance (100 mHz) and R_p increased. The maximum R_p significantly and

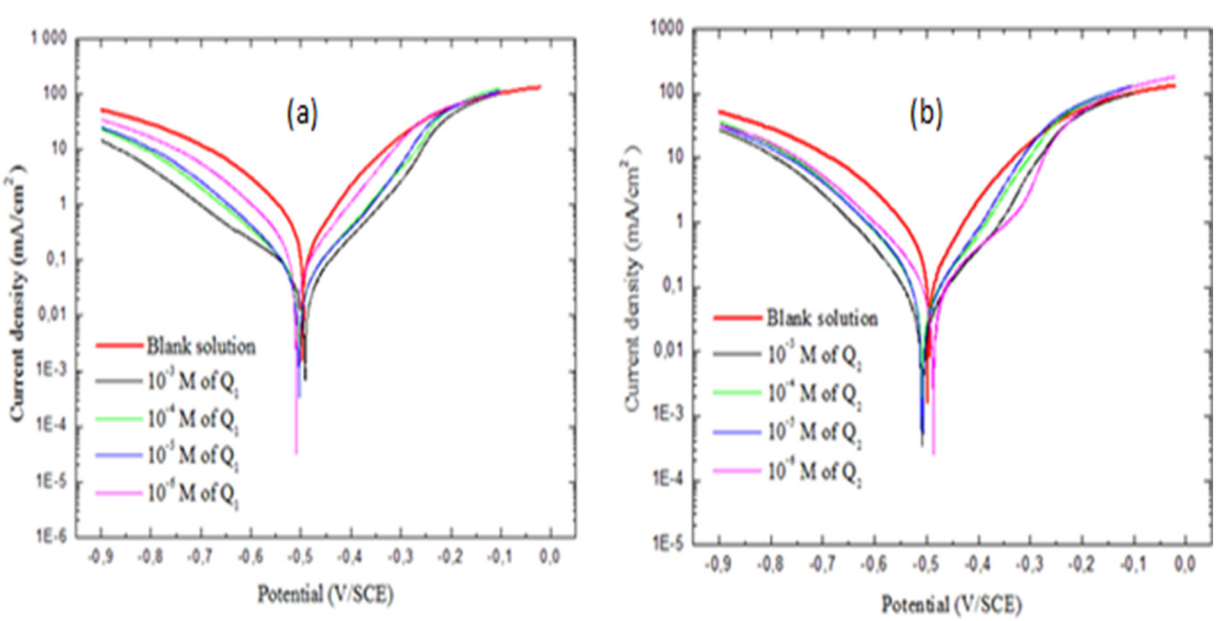

Fig. 1. Steel polarization curves in 1 M HCl medium with and without the addition of (a) Q_1 and (b) Q_2 at 298 K.

impedance values are obtained for the sample dipped in solution containing 10^{-3} M Q_1 and Q_2. The values of double layer capacitance (C_{dl}) are calculated according to formula 5, and the results are shown in Table 5.

$$C_{dl} = Q^{1/n_{dl}} \times R^{(1-n_{dl})/n_{dl}} \quad (5)$$

with n_{dl} is the degree of heterogeneity

Another important thing was observed that C_{dl} values decrease after adding Q_1 and Q_2. This also indicates that the thickness of the double layer increase with Q_1 and Q_2 concentration, which is well explain by this formula (6) [18]:

$$C_{dl} = \frac{\varepsilon_0 \varepsilon}{d} S \quad (6)$$

where, ε_0 is the permittivity of space, ε is the local dielectric constant, d is the film thickness and S is the surface area. From formula it is found that C_{dl} is directly proportional to ε and inversely proportional to d. The C_{dl} value was decreased due to decrease in local dielectric constant because of replacement of water molecules (higher ε value) by the inhibitor molecules (lower ε value). The increase in thickness (d) of the electrical double layer was observed with increase in concentration of Q_1 and Q_2 which also play an important role in decrease of C_{dl} value [19].

It can be clearly seen from Fig. 2 that the increase in Q_1 and Q_2 concentration results in the increase of corrosion inhibition performance. The maximum corrosion inhibition performance was obtained at 10^{-3} M Q_1 and Q_2. These organic compounds (Q_1 and Q_2) include many polar groups and aromatic rings. The coordination between the lone pair electrons of heteroatoms, such as O, N, and empty orbital of metal cations, and the interaction between the electrons in aromatic rings with empty orbital of metal cations is the mechanism of Q_1 and Q_2 adsorption on the *MS* surface. The organic molecules adsorption on the *MS* surface restricts the access of the corrosive agents to the actives sites.

3.4. Effect of temperature

The stability of a corrosion inhibitor in an aggressive medium at given use temperatures is very important for its application. In acid stripping, the role of the inhibitors is to protect the metal installations against acid attacks. These stripping operations are usually carried out at high temperatures [20]. In our case, the study of the influence of temperature (298–328 K) on the corrosion inhibition rate of MS for the two 8-hydroxyquinolines was carried out potentiodynamic polarization. The cathodic and anodic polarization curves of steel in 1 M HCl medium in the absence and in the presence of Q_1 and Q_2 at 10^{-3} M are shown in Fig. 5. The values of corrosion current densities (i_{corr}), corrosion potentials of steel (E_{corr}), and the inhibitory performance of Q_1 and Q_2 as a function of temperature are given in Table 6. We note that the increase in temperature causes an increase in i_{corr} and the inhibitory performance decreases throughout the temperature range studied [21]. It also shows that Q_1 and Q_2 retain their inhibitory properties for all temperatures studied. However, in the case of the inhibitor Q_1, which proved to be the best inhibitor of this family, the decrease in the inhibitory performance is less important and reaches 82.6% at 328 K.

3.5. Kinetic/thermodynamics considerations

The thermodynamic parameters specifically activation energy (E_{act}), entropy of activation (ΔS_{act}) and enthalpy of activation (ΔH_{act}) for corrosion reaction at 10^{-3} M for Q_1 and Q_2 were calculated from Arrhenius and transition state plot. The activation energy was calculated by Arrhenius formula (7).

$$i_{corr} = A \exp\left(\frac{-E_a}{RT}\right) \quad (7)$$

and other two parameters ΔH_{act} and ΔS_{act} were calculated utilizing the transition state formula:

$$i_{corr} = \frac{RT}{Nh} \exp\left(\frac{\Delta S_{act}}{R}\right) \exp\left(\frac{-\Delta H_{act}}{RT}\right) \quad (8)$$

where, R, T, A, N & h are universal gas constant, absolute temperature, pre-exponential factor, Avogadro number and plank constant, respectively. The i_{corr} values were obtained from the extrapolation of Tafel plot at different temperature with and without adding Q_1 and Q_2 molecules. Here, i_{corr} values consider as a corrosion rate. From the Arrhenius plots, the $Ln\ i_{corr}$ against $1000/T$ at the optimal concentration of Q_1 and Q_2 is shown in the Fig. 6.

From Fig. 6 showing a curve in a straight line and having a slope equal to $-E_a/RT$, we have calculated the energy value of Ea. Another plot of $Ln\ (i_{corr}/T)$ vs. $1000/T$ show a straight line curve (presented in Fig. 7) with a slope and intercept those are equal to $-\Delta H_{act}/R$ and $Ln\ (R/Nh) + \Delta S_{act}/R$, respectively.

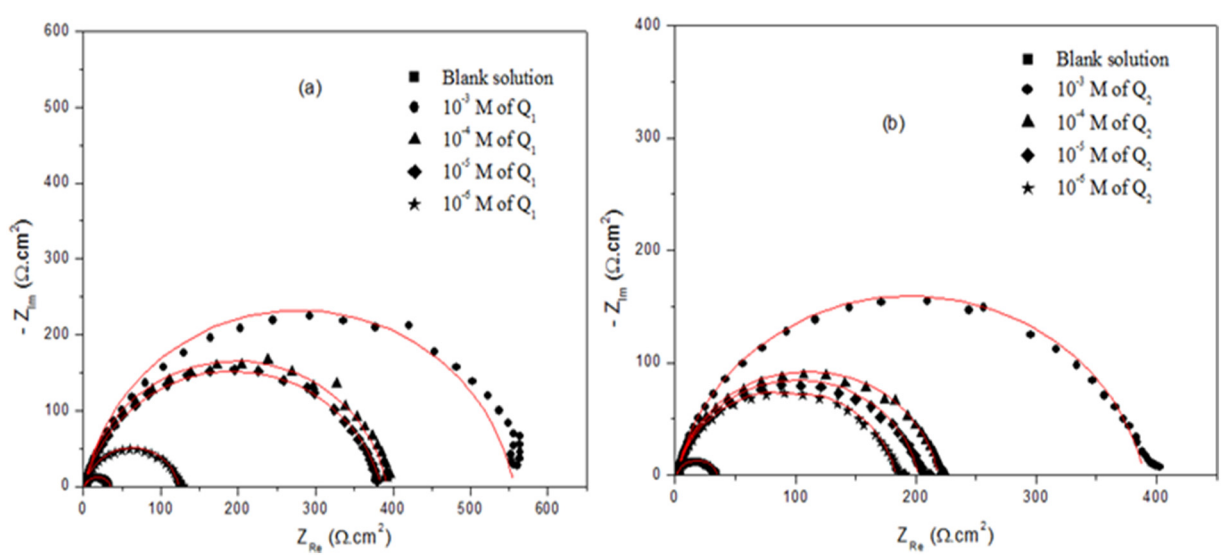

Fig. 2. Impedance spectra of MS corrosion in 1 M HCl with and without different concentrations of (a) Q_1 and (b) Q_2 at 298 K.

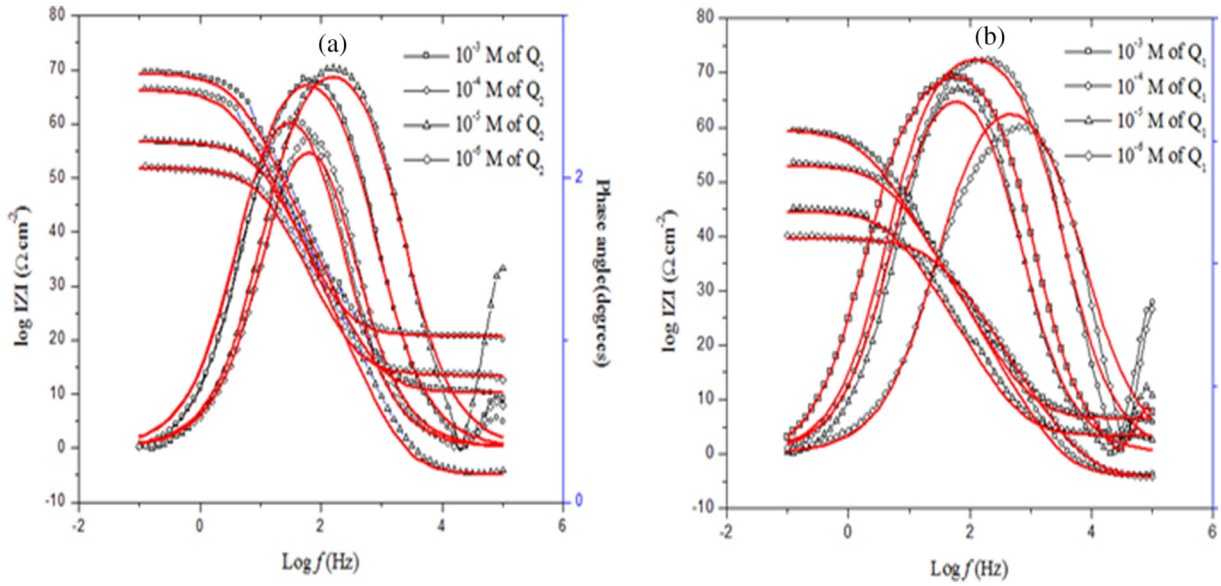

Fig. 3. Phase and Bode plot for MS corrosion in 1 M HCl without inhibitor (a), and in the presence of (b) Q_1 and (c) Q_2.

The values of ΔH_{act} and ΔS_{act} listed in Table 7, which were calculated from the slope and intercept. From Table 7 and Fig. 6, it can be seen that the activation energy (E_{act}) in presence of both Q_1 and Q_2 is higher than the blank solution on *MS* corrosion which indicates the metal dissolution decreases in acidic medium because of increase in the energy barrier for mild steel corrosion.

Meanwhile the activation entropy (ΔS_{act}) value increases in addition of Q_1 and Q_2 compared to given acid solution and the values were found in negative. The higher ΔS_{act} values in presence of Q_1 and Q_2 signified the entropy of the solvent increases. This may be occur due to desorption of large numbers of water molecule which were already adsorbed on the metal surface and less disorder larger Q_1 and Q_2 molecules adsorbed on the *MS* surface [22,23].

3.6. Adsorption isotherm

The adsorption isotherm is providing some useful information regarding corrosion mechanism. Many factors are control the adsorption process, like nature of the metal surface and its charge, solvent and other ionic species adsorption, electrochemical potential between metal-solution interface, temperature during corrosion reaction. The adsorption process is divided into two categories. Frist one is chemisorption, it occurs when the direct interaction between adsorbed inhibitors molecule and metal surface like donor-accepter type interaction. Chemical adsorption implies the charge sharing or charge transfer from adsorbates (inhibitor molecule) to the metal surface and forms a very strong metal-inhibitor coordinate bond.

These types of interaction are basically irreversible in nature. The second one is physisorption, here the inhibitor molecules adsorb on the metal surface through week undirected interaction which is basically formed due to the electrostatic interaction between metal and inhibitor's solution interface [24]. To evaluate the adsorption isotherm nature, several adsorption isotherms were tested. It was observed that the adsorption of Q_1 and Q_2 on *MS* in 1 M HCl medium obey the Langmuir adsorption isotherm formula:

$$\frac{C_{inh}}{\theta} = \frac{1}{K_{ads}} + C_{inh} \tag{9}$$

where K_{ads}, θ and C_{inh} are inhibitor adsorption constant, degree of surface coverage and Q_1 and Q_2 concentration, respectively. Values of $\theta = \eta/100$ was taken from weigh loss measurement. The plot of C_{inh}/θ vs C_{inh} gave a straight line curve (Fig. 8) having $1/K_{ads}$ intercept and the correlation coefficient (R^2) values for Q_1 and Q_2 are 1.00 and 0.99, respectively.

The straight line and strong correlation coefficient value indicate the Langmuir adsorption isotherm the best fitted with experimental data. The ΔG_{ads}^{o} value was calculated utilizing the formula:

$$\Delta G_{ads}^{\circ} = -RTLn(55.55K_{ads}) \tag{10}$$

where, T is the temperature, R is the gas constant. The values of K_{ads} is represented here in L mol^{-1}, thus in this formula the concentration of water is taken in L mol^{-1} (55.5 mol/L). In general, when the obtained ΔG_{ads}^{o} values of inhibitor lie in the order of −20 kJ mol^{-1} or even lower (more positive), it satisfies the physisorption of inhibitor on metal surface. While the ΔG_{ads}^{o} values around −40 kJ mol^{-1} or higher (more negative) are associated with chemisorption [25]. The obtained

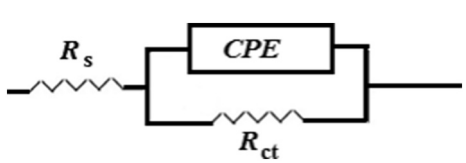

Fig. 4. The equivalent circuit corresponding to the impedance spectra.

Table 5
Parameters evaluated from Nyquist and Bode diagrams for MS corrosion in 1 M HCl in the presence and absence of various concentrations of Q_1 and Q_2 at 298 K.

Medium	C (M)	R_s (Ω cm^2)	R_{ct} (Ω cm^2)	C_{dl} (μF cm^{-2})	n_{dl}	Q (μF S^{n-1})	η_{EIS} %
Blank	00	1.22	33.97	121.0	0.82	315.0	–
Q_1	10^{-3}	1.57	554.7	31.6	0.88	49.5	93.1
	10^{-4}	1.40	390.5	37.3	0.89	57.9	90.2
	10^{-5}	1.51	382.8	42.7	0.85	77.2	90.0
	10^{-6}	1.98	121.0	55.8	0.89	94.9	68.6
Q_2	10^{-3}	1.41	388.5	61.4	0.87	97.3	90.1
	10^{-4}	1.42	217.0	59.8	0.89	92.0	82.2
	10^{-5}	1.55	200.3	60.1	0.89	96.0	81.0
	10^{-6}	1.58	181.6	56.2	0.88	295.0	79.0

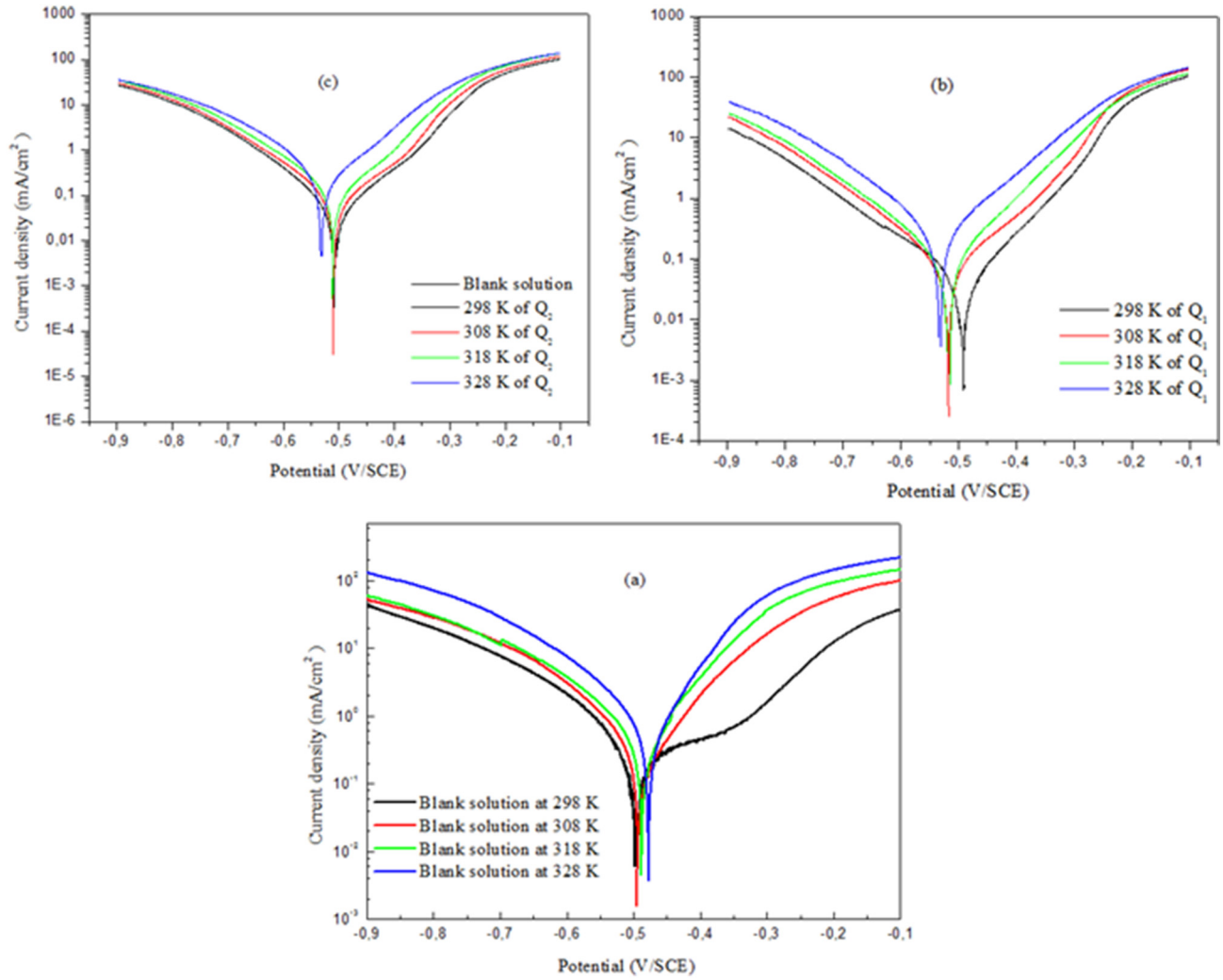

Fig. 5. Effect of temperature on the polarization curves of (a) MS in 1 M HCl and in the presence of (b) Q_1 and (c) Q_2.

ΔG_{ads}^{o} values of Q_1 and Q_2 are −46.3 kJ mol^{-1} and −42.6 kJ mol^{-1} for Q_1 and Q_2, respectively (Table 8). The range of ΔG_{ads}^{o} values above indicates the contribution of the chemisorption mechanism [26,27].

3.7. UV–Visible spectroscopy

In order to confirming the possibility of the formation of 8-hydroxyquinoline derivatives-Fe complex, UV–Visible absorption spectra obtained from 1 M HCl solution containing 10^{-3} M of Q_1 and Q_2 before and after 48 h of *MS* immersion are shown in Fig. 9. The electron absorption bands of compounds solutions (Figs. 9(a and b)), before immersion of *MS* in 1 M HCl solution show visible absorption bands

Table 6
Values of the corrosion current density and the inhibition performance in the presence of 10^{-3} M of Q_1 and Q_2 at different temperatures.

Medium	T (K)	$-E_{corr}$ (mV/SEC)	i_{corr} (μA/cm²)	Tafel slopes (mV/dec)		η_{PDP} (%)
				$-\beta_c$	β_a	
Blank	298	498	983	92	104	–
	308	491	1200	184	112	–
	318	475	1450	171	124	–
	328	465	2200	161	118	–
Q_1	298	508.6	50.41	146.4	45.8	94.8
	308	515.5	72.78	131	40.9	92.5
	318	533.9	82.11	116.4	42.2	91.6
	328	529.6	170.4	101.6	42.6	82.6
Q_2	298	507.2	53.43	103	175	92.2
	308	508.2	90.65	116.1	45.1	90.7
	318	508.6	126.83	116.6	206.6	87.0
	328	531.1	311.2	119.5	58.5	68.0

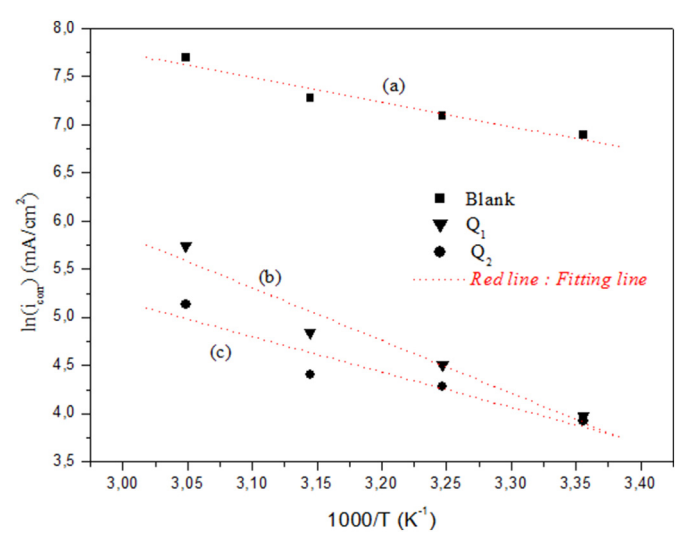

Fig. 6. Arrhenius plots for MS corrosion in 1 M HCl in the absence (a) and presence of (b) Q_2 and (c) Q_1 at 10^{-3} M.

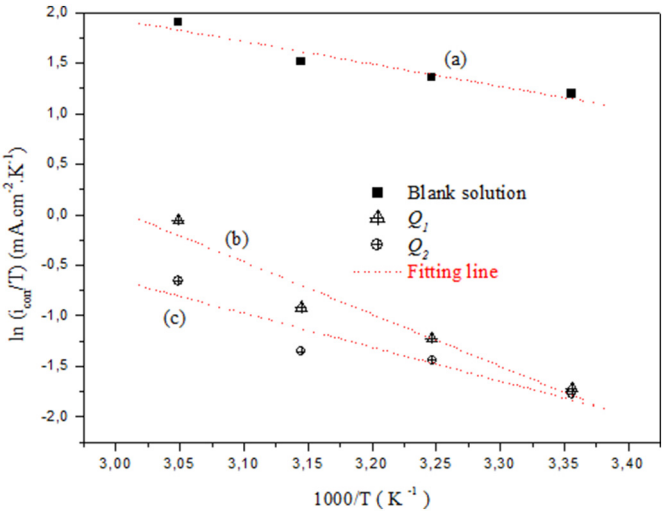

Fig. 7. Transition state plots for Q_1 and Q_2 in 1 M HCl medium on MS corrosion.

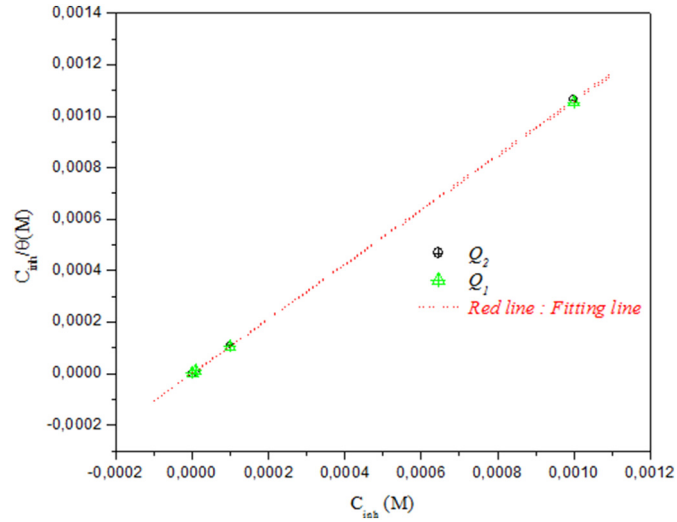

Fig. 8. Langmuir adsorption isotherm plots for the adsorption of Q_1 and Q_2 on MS corrosion surface in 1 M hydrochloric acid.

256.67 nm, and 258.81 nm respectively for Q_1 and Q_2. This stripe may be assigned to the π-π* transition implying the ensemble, electronic structure system of Q_1 and Q_2 with an important charge transfer character. However, after 48 h of immersion of specimen *MS* panels in aggressive solution (Figs. 9(a and b)), the absorption bands λ_{max} underwent a bathochromic shift from 256.67 nm to 258.81 nm and from 251.97 nm to 254.42 nm respectively for Q_1 and Q_2. A change in the position of the absorption maximum λ_{max}, show the formation of a complex between the two species in solution as described in the collected works. Our experimental results are suitable evidence for the chance of the formation of a complex among Fe^{2+} and Q_1 and Q_2 in molar hydrochloric acid [28].

3.8. Scanning electron microscopy (SEM)

The *MS* panels surface morphology analysis utilizing *SEM* is a very essential equipment to study the surface of corroded and uncorroded metal. The corrosion inhibition ability of Q_1 and Q_2 are directly judged by the matching of *MS* surface morphology with Q_1 and Q_2 (10^{-3} M) and without (in molar HCl solution). The *SEM* images were taken after 6 h immersion of metal coupon in given solution. The first image (Fig. 10a) shows the badly damage surface which is without inhibitor metal. In this morphology, the enormous numbers of ups and down are spread all over the metal surface. But in Fig. 10 2nd and 3rd image display the much cleaner and smoother surface than 2st image [29].

This image indicates that Q_1 and Q_2 are adsorbed on the surface of MS panels and protect the metal from aggressive media, and it can also see that Q_1 show better effect than Q_2, due to well protective layer formation.

3.9. Theoretical computation

3.9.1. Determination of the quantum chemical parameters of the molecules tested

The quantum chemical computation based *DFT* were carried out by Gaussian 09 program at the *B3LYP/6-31G* (*d*, *p*) system to study the effects of the organic molecular structures, electronic properties of studied molecules on the inhibition performance, and explain the type of effect of the corrosion operation [30]. The geometry of optimized molecules and the frontier molecular orbital (*FMO*) density distributions of the neutral compounds Q_1 and Q_2 were shown in Fig. 11. The *HOMO* mostly distributed around the hydroxyquinoline heterocyclic for the two studied compounds Q_1 and Q_2, This motive is considered an electron donating group to supply electrons to the unoccupied d-orbital of Fe to form coordination bonds. While the *LUMO* was localized on the hydroxyquinoline for Q_1 but it is distributed on methyl nitrobenzoate for Q_2, here the electron-withdrawing group (NO_2) attracts the electrons towards it.

The parameters such as energy of frontier molecular electrons, energy gap ($\Delta E_{gap} = E_{LUMO} - E_{HOMO}$), electronegativity ($\chi$), electrophilicity ($\omega$) and nucleophilicity ($\varepsilon$) index, hardness ($\eta$), fraction of electrons transferred from the inhibitor to the surface of the metal (ΔN_{110}) and the total energy (*TE*) are recorded in Table 9. These parameters are expressed in the following formulas [31]:

$$IP = -E_{HOMO} \tag{11}$$

$$EA = -E_{LUMO} \tag{12}$$

$$\eta = \frac{\Delta E_{gap}}{2} \tag{13}$$

$$\chi = \eta + EA \tag{14}$$

$$\omega = \frac{\chi^2}{2\eta} \tag{15}$$

$$\varepsilon = \frac{1}{\omega} \tag{16}$$

$$\Delta N_{110} = \frac{\phi - \chi_{inh}}{2(\eta_{Fe} + \eta_{inh})} \tag{17}$$

Table 7
Activation parameters of MS corrosion in 1 M HCl medium without and with addition of Q_1 and Q_2 at 10^{-3} M.

Medium	E_a (KJ mol^{-1})	ΔH_a (KJ mol^{-1})	$-\Delta S_a$ (J mol^{-1} K^{-1})
Blank	21.02	18.45	126.08
Q_1	30.47	27.87	119.24
Q_2	45.47	42.87	68.52

Table 8
Thermodynamic parameters of adsorption of Q_1 and Q_2 on MS at 298 K.

Inhibitor	K_{ads} (mol^{-1})	R^2	ΔG_{ads} (kJ mol^{-1})
Q_1	2,399,427	1.00	−46.3
Q_2	535,790	0.99	−42.6

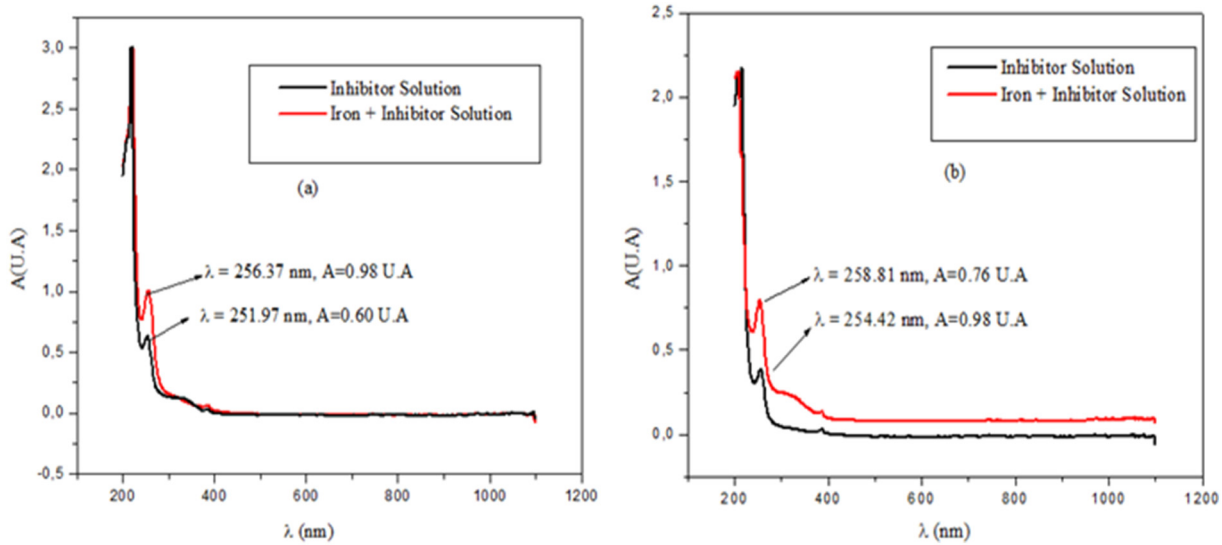

Fig. 9. UV–visible spectra of 1 M HCl solution containing 10^{-3} M of (a) Q_1 and (b) Q_2 before (black) and after (red) After 6 h of MS immersion.

The ϕ means the work function; the value ΔN is more appropriate for the use of the work function (ϕ). In the literature, the value obtained for the function ϕ is 4.82 eV for the surface Fe (110) [32]. The hardness value of iron (η_{Fe}) is zero considering $IP = EA$ for the metallic bulk [33].

In this work, we discussed the various results obtained theoretically for the two neutral and protonated forms of the studied molecules Q_1 and Q_2. First, we started by neutral forms.

The two indices E_{HOMO} and E_{LUMO} have related the donor and acceptor capacities of the electrons of a substance, respectively. Indeed, the molecules that have high values of E_{LUMO} and E_{HOMO}, they are admirable corrosion inhibitors. In this context, the high value of *HOMO* energy translates that the molecule studied possesses a great capacity to give electrons to the metallic surface, [34] and in this investigation they have the order -5.818 $Q_1 > -6.074$ Q_2 that is, the molecule Q_1 has a capacity to offer electrons more than the molecule Q_1. This can be linked to the chlorine donor electron group (—Cl). In addition, the energy gap is another important parameter that describes the interaction between Q_1 and Q_2 and Metallic Iron. Generally, the molecule that has the lowest value of ΔE_{gap} is more stable and considered better inhibitor [35]. The studied Q_1 and Q_2 inhibitors have small deference's of ΔE_{gap} and that was of 3.184 eV and 3.788 eV, respectively. Concerning the electronegativity index (χ) the molecule that possesses the lowest χ, it is related with higher electron donating tendency indeed, the inhibition performance is important with the molecule has a high value of (χ). From Table 9 the values of χ are ranked as follows: $Q_1 > Q_2$, this result supports the experimental data. The values of the fraction of electrons transferred (ΔN_{110}) are also grouped in Table 9. These values show that the inhibition performance resulting from electron donation agrees with Lukovit's study (ΔN_{110}<3.6> [36]. The inhibition performance increases with electron donation power of these molecules studied to

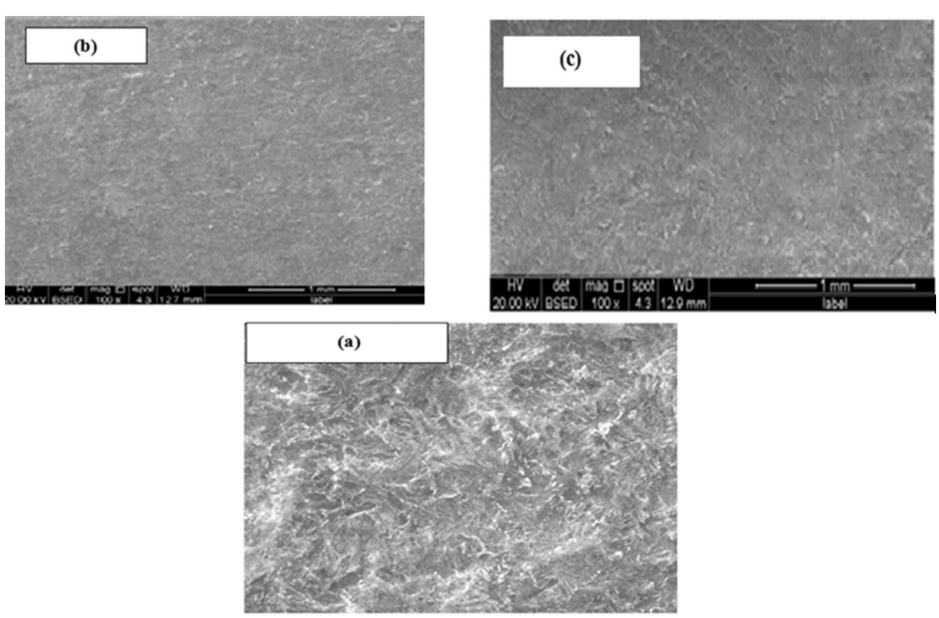

Fig. 10. SEM image of MS before (a) and after immersion for 6 h in 1 M HCl with 10^{-3} M of (b) Q_1 and (c) Q_2.

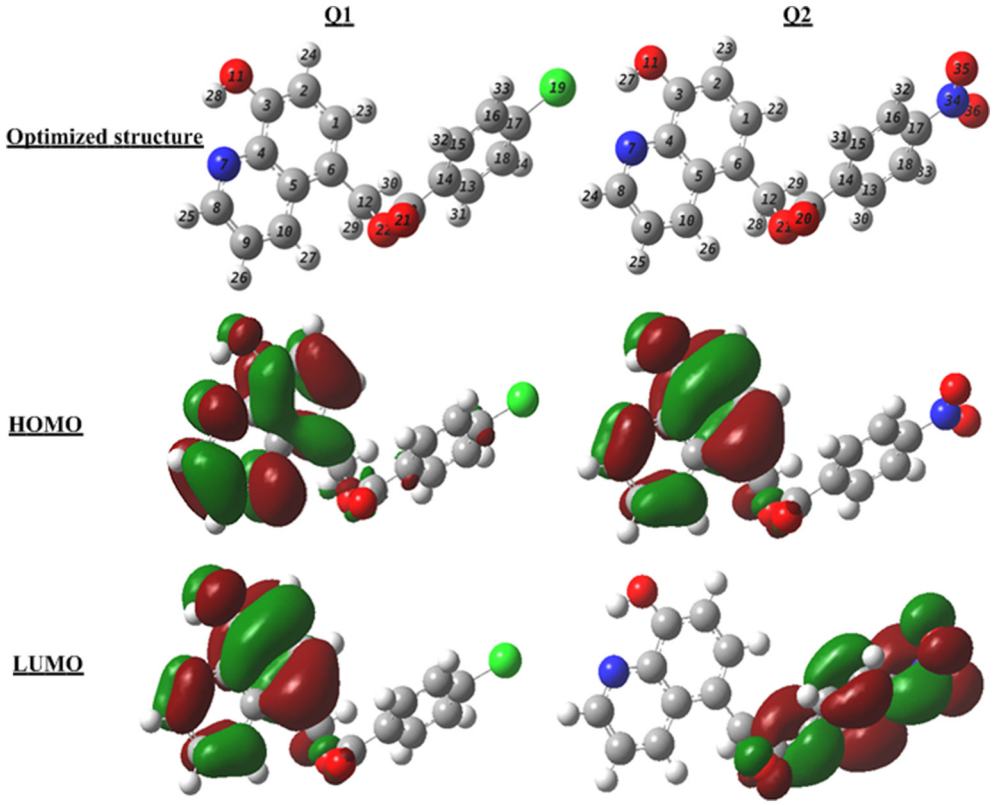

Fig. 11. Optimized structures and the FMO density distributions of the investigated the neutral compounds Q_1 and Q_2: HOMO and LUMO.

offer electrons to the iron surface [37]. The ΔN_{110} values of Q_1 and Q_2 are classified according to the following sequence: $\Delta N_{110}(Q_1) > \Delta N_{110}(Q_2)$. To measure the electron-accepting ability of a molecule we use the electrophilicity (ω) index, on the contrary, we find the nucleophilicity (ε) index. Indeed, a molecule with a lower value of ε and higher value of ω is possible to behave as good corrosion inhibitor [38]. From Table 9, it is clear that the values of nucleophilia and electrophilia are confirmed by experimental measurements.

Concerning the protonated forms the studied molecules exist in the cationic form in an acidic middle [39]. For it, we have protonated the nitrogen atom (N7), which belongs to the quinoline heterocyclic and considered as the most available site for protonation. Quantum chemical indices are also represented in Table 9.

From Table 9, E_{HOMO} values of the tested compounds are displaced to more negative values than that of the E_{HOMO} values of the neutral molecules Q_1 and Q_2. This indicates that these two molecules can take electrons from Fe (110) [40]. The values of ΔE_{gap}, χ, T_E and ω show that the reactivity of the protonated molecules increases remarkably. So, the protonated molecules interact more easily with the metal of the Fe.

The different quantum chemical parameters for protonated and non-protonated Q_1 and Q_2 molecules have supported the results obtained experimentally.

Table 9
Quantum chemical calculation data of Q_1 and Q_2 neutral and protonated forms for the *B3LYP/6-31G (d,p)* method.

Parameters	Neutral molecules		Protonated molecules	
	Q_1	Q_2	$Q_1(N7H)^{+1}$	$Q_2(N7H)^{+1}$
E_{LUMO} (eV)	−1.997	−2.286	−6.549	−6.587
E_{HOMO} (eV)	−5.818	−6.074	−9.062	−9.856
ΔE_{gap} (eV)	3.184	3.788	2.513	3.270
η (eV)	1.592	1.894	1.256	1.635
χ (e·V)	3.589	4.180	7.805	8.222
ω	4.045	4.612	24.250	20.673
ε	0.247	0.216	0.041	0.048
ΔN_{110}	0.386	0.169	−1.188	−1.040
T_E (μa)	−1395.68	−1140.59	−1396.087	−1140.988

3.9.2. Location of active centers

The active centers of Q_1 and Q_2 were further confirmed by the etude of molecular electrostatic potential (*MEP*), the density of the atomic charge of Mulliken and the Fukui parameters. First of all, *MEP* is allowing the electron density visible and determined the sites of electrophilic and nucleophilic attack for a molecule [41]. The total density distribution in *MEP* shows that the red regions (negative) are represented on the nucleophilic attack, while the blue regions (positive) are responsible for the electrophilic attack. In Fig. 12 it is clear that the total electron density for the negative regions is distributed over the oxygen atoms that are available for nucleophilic attack while blue regions are corresponding to the *LUMO* orbital distribution of studied substances.

In addition, Fukui indices are good indicators utilized to precise the local reactivity of a molecule. These indices or functions are calculated as follows:

$$f\left(\vec{r}\right) = \left(\frac{\partial \rho\left(\vec{r}\right)}{\partial N}\right)_{V\left(\vec{r}\right)}. \tag{18}$$

The functions of Fukui $f(\vec{r})^{+}$ and $f(\vec{r})^{-}$ are utilized to establish the sites responsible for the electrophilic and nucleophilic attack of

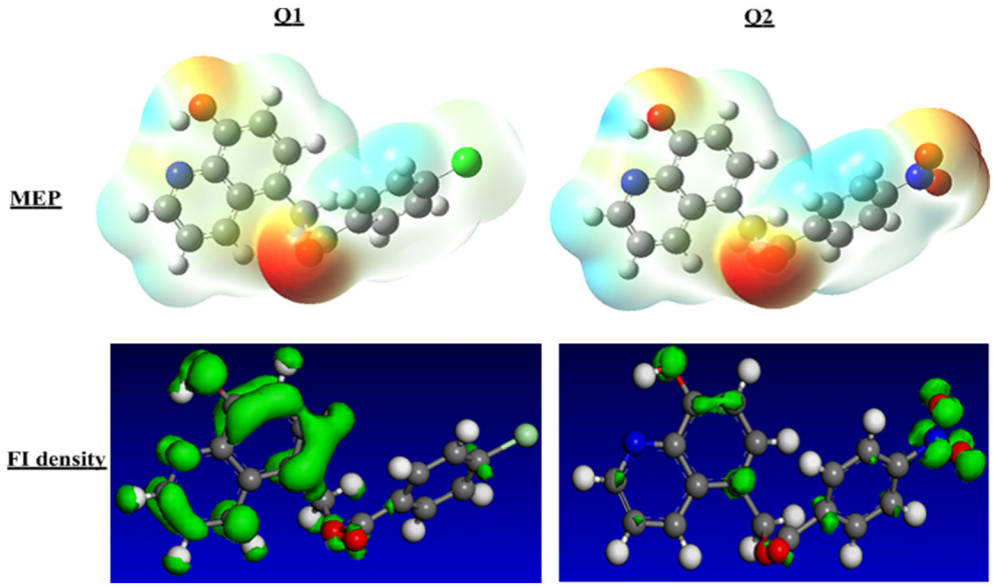

Fig. 12. Density distribution of MEP and FI for both inhibitors Q_1 and Q_2.

inhibitory molecules. They are calculated by formulas (19) and (20) [42]:

$$f_i\left(\vec{r}\right)^+ = q_i(N+1) - q_i(N) \tag{19}$$

$$f_i\left(\vec{r}\right)^- = q_i(N) - q_i(N-1) \tag{20}$$

where $q_i\,(N+1)$, $q_i\,(N)$, $q_i\,(N-1)$ are charge values of atom i for cation, neutral and anion, respectively.

The calculated Fukui indices of inhibitors studied are shown in Fig. 12 and grouped in Table 10. These indices are calculated by the Materials Studio 8 software from Biovia-Accelrys Inc., utilizing the Dmol^3 module. The calculations are executed utilizing the correlation *BOP* function and the digital double polarization (*DNP*).

Table 10
Values of electron donor and acceptor centers of inhibitory molecules (Q_1 and Q_2).

Atom	Mulliken charge		$f(\vec{r})^+$		$f(\vec{r})^-$	
	Q_1	Q_2	Q_1	Q_2	Q_1	Q_2
C2	−0.116	−0.100	0.027	−0.001	0.067	0.070
C3	0.305	0.337	0.046	0.010	0.039	0.040
C4	0.132	0.169	0.013	0.006	0.037	0.028
C6	0.000	0.019	0.032	−0.013	0.086	0.084
N7	−0.369	−0.386	0.074	0.009	0.024	0.028
C8	0.071	0.115	0.048	0.007	0.031	0.032
O11	−0.428	−0.454	0.050	0.015	0.124	0.125
C12	0.076	0.130	0.000	−0.016	−0.005	0.000
C17	0.008	0.179	0.011	0.001	−0.000	0.004
Cl19	−0.072	–	0.049	–	0.038	–
C19	–	0.544	–	0.031	–	−0.014
C20	0.521	–	0.009	–	−0.012	–
O20	–	−0.389	–	0.063	–	0.035
O21	−0.377	−0.493	0.042	0.016	0.031	0.017
O22	−0.487	–	−0.015	–	0.019	–
N34	–	0.377	–	0.082	–	0.001
O35	–	−0.341	–	0.181	–	0.017
O36	–	−0.343	–	0.181	–	0.020

From Fig. 12 and Table 10 the atoms C3, N7, C8 and O11 for Q_1 and the atoms O20, N34, O35 and O36 for Q_2 are available to accept electrons. These atoms have high values of $f(\vec{r})^+$. While the atoms C2, C3, C6, and O11 are responsible for giving electrons to the metal of the Fe to form coordination bonds. This results in the high values of $f(\vec{r})^-$. So, all these centers of the studied molecules may be responsible for the inhibitory performance.

The atomic charge of Mulliken is another descriptor that determines the local reactivity of a molecule. The various atomic charges of substances studied are grouped in Table 10. Atoms that carry higher negative charges; they are as electron donors (nucleophilic centers). So, The C2, N7, O11 and O21 atoms of Q_1 and the atoms N7, O11, O20, O21, O35 and O36 of Q_2 are active sites capable of delivering electrons as they interact with the metal surface. While, While, the carbon atoms C3, C4 and C20 of Q_1 and the atoms C1, C2, C4, C8, C12, C17, C19 and N34 of Q_2 carry a high density of positive charges. This shows that these atoms are considered electron acceptor active sites.

3.10. Simulation by Monte Carlo

To know adsorption configurations and interactions between inhibitors and the metal surface we performed the Monte Carlo simulation of the inhibitory molecules on the area of Fe (110). This simulation is made in an area of (26.894 × 26.894 × 22.134 Å) with periodic boundary conditions, a super cell of (7 × 7), a vacuum of 40 Å and we studied six layers of iron to ensure that the area depth was greater than the non-cut utilized in the simulation [43]. The interaction energy for the system the Fe (110)/inhibitory molecule is calculated by the relation (21):

$$E_{\text{int}} = E_{Total} - \left(E_{Surface} + E_{Inhibitor}\right) \tag{21}$$

Where the total energy of the area and the inhibitor molecule is expressed by E_{total}, $E_{surface}$ is the surface energy without the inhibitor and the inhibitor is the energy of the fixed inhibitor at the area of the Fe. The binding energy ($E_{binding}$) of the inhibitory molecule is presented as following:

$$E_{binding} = -E_{\text{int}}. \tag{22}$$

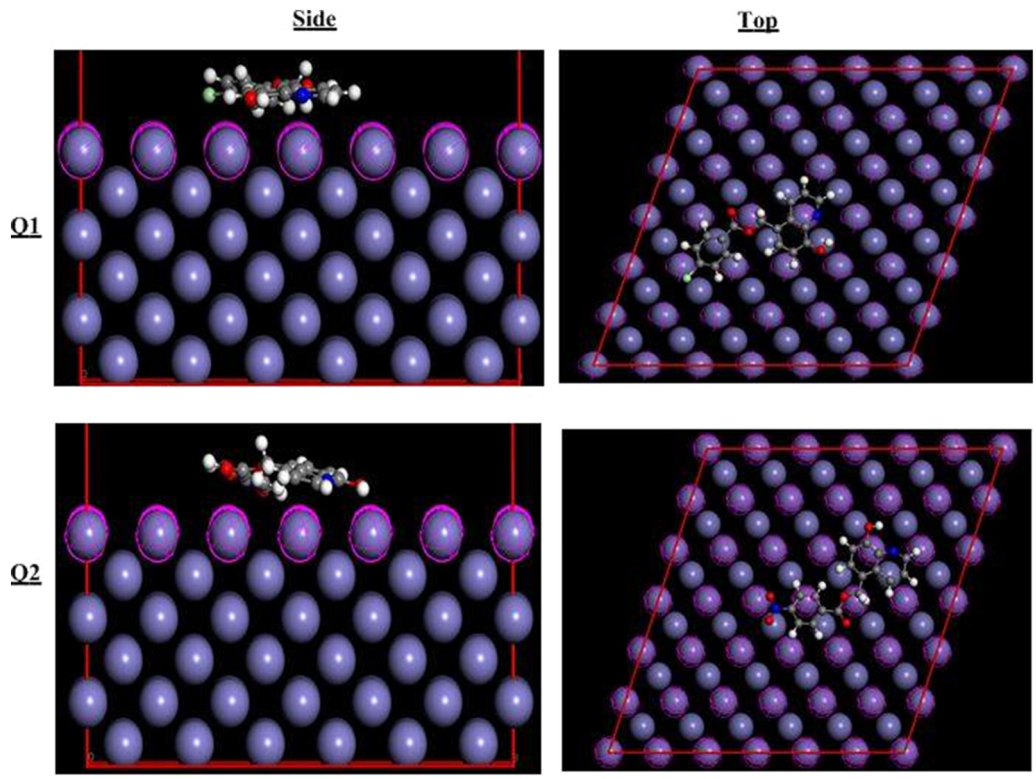

Fig. 13. Side and top views of most stable adsorption configuration for Fe (110)/Q_1 and Q_2 interface obtained through the MC simulation.

Table 11
Outputs and descriptors for the lowest adsorption configurations for Fe (110)/(Q_1 and Q_2) system. (All values in Kcal/mol).

Inhibitor	Total energy	Adsorption energy	Rigid adsorption energy	Deformation energy	$\frac{dE_{ad}}{dE_i}$
Fe(110)/Q_1	13.269	−112.840	−56.145	−56.695	−112.840
Fe(110)/Q_2	41.087	−112.800	−55.484	−57.316	−112.800

Fig. 13 shows that the adsorption actives sites on the iron surface (110) are the lone pair of electrons on the atoms (N, O, and Cl) and π-electrons of aromatic cycles for inhibitor molecules Q_1 and Q_2. These two inhibitors are adsorbed in a planar manner onto the *Fe (111)* as well as the close contacts between those.

The different energy values in Kcal/mol of the most stable configuration of Q_1 and Q_2 are tabulated in Table 11. In addition, the rigid adsorption energy (*R.A.E*) is defined as the energy relaxed when the no relaxed molecule. For the energy released by the adsorbed inhibitor molecules, Q_1 and Q_2 on the iron surface (110) is presented by deformation energy (D_E). The ($\frac{dE_{ad}}{dE_i}$) is the energy required to remove adsorbents from the metal area.

From Fig. 12 we have observed that all E_{ads} values for Fe (110)/Q_1 and Q_2 system is negative, which indicate that the molecules Q_1 and Q_2 are strongly and quickly adsorbed on the area Fe (110) [44]. The adsorption energy value of the Q_1 (−112.800Kcal/mol) in equilibrium configuration, is higher than that of Q_2 (−112.840 Kcal/mol). This indicates that the Q_1 molecule adsorbs better than the Q_2 molecule on the iron surface. We say that this result overlaps with the experimental

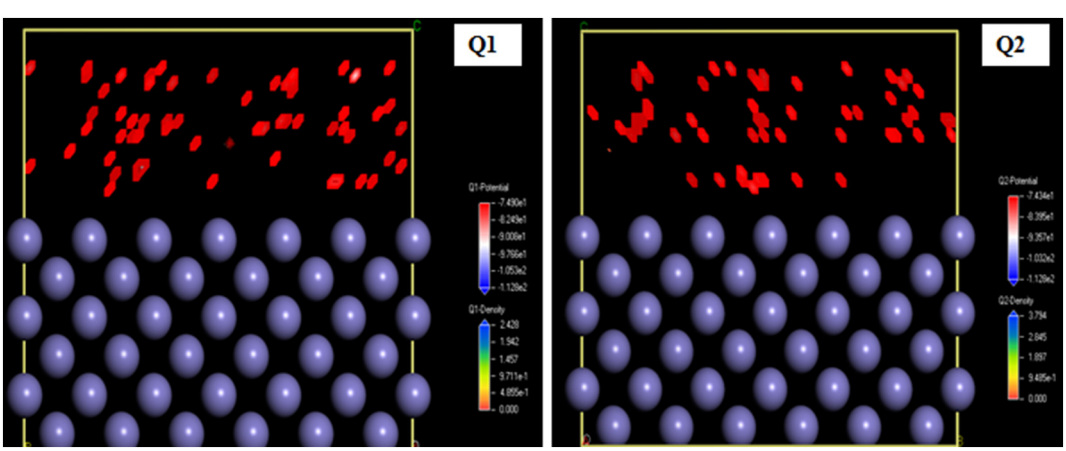

Fig. 14. Adsorption density field of Q_1 and Q_2 inhibitor molecules on the Fe (1 1 0) substrate.

data. Fig. 13 shows from the minimum to the maximum values of the electrostatic potential and the adsorption density for Fe (110)/Q_1 and Q_2 interface.

From Fig. 14 it is obvious that the change in the colors of the isosurface of the substances studied results in the maximum and minimum values that are related to the field of electrons mapped and *MEP*. The electron density distribution for the two compounds studied means more likely adsorption sites for these molecules Q_1 and Q_2 on the Fe (110) metal area.

4. Conclusion

Compound Q_1 exhibits the best corrosion inhibition performance that compound Q_2 which is confirmed by electrochemical studies and weight loss. From the Polarization results, it could be confirmed that both the polymers are mixed type corrosion inhibitor and their adsorption obey the Langmuir Adsorption isotherm. The UV–Visible studies clearly reveal the formation of a complex that may also be responsible for the observed inhibition. *SEM* images also confirm the inhibitor adsorption process and reduction in the surface damage of MS due to corrosion. The effect of the strong protective power of inhibitory molecules Q_1 and Q_2 is attributed by chemical quantum parameters. The theoretical parameters founded are a good correlation with the experimental data. Monte Carlo simulations show the great interaction between the tested Q_1 and Q_2 compounds and the metal surface of the iron, and the Q_1 molecule is better adsorbed on the Fe (110) surface than the Q_2 molecule.

Appendix A. Supplementary data

Supplementary data to this article can be found online at https://doi.org/10.1016/j.molliq.2018.11.104.

References

[1] C. Verma, M.A. Quraishi, A. Singh, 2-Amino-5-nitro-4,6-diarylcyclohex-1-ene-1,3,3-tricarbonitriles as new and effective corrosion inhibitors for mild steel in 1 M HCl: experimental and theoretical studies, J. Mol. Liq. 212 (2015) 804–812.

[2] C. Verma, E.E. Ebenso, I. Bahadur, I.B. Obot, M.A. Quraishi, 5-(Phenylthio)-3H-pyrrole-4-carbonitriles as effective corrosion inhibitors for mild steel in 1 M HCl: experimental and theoretical investigation, J. Mol. Liq. 212 (2015) 209–218.

[3] S.M. Tawfik, Corrosion inhibition efficiency and adsorption behavior of *N*,*N*-dimethyl-4-(((1-methyl-2-phenyl-2,3-dihydro-1H-pyrazol-4-yl)imino)methyl)-*N*-alkylbenzenaminiumbromide surfactant at carbon steel/hydrochloric acid interface, J. Mol. Liq. 207 (2015) 185–194.

[4] M. El Faydy, T. Djassinra, S. Haida, M. Rbaa, K. Ounine, A. Kribii, B. Lakhrissi, Synthesis and investigation of antibacterial and antioxidants properties of some new 5-subsituted-8-hydroxyquinoline derivatives, J. Mater. Environ. Sci. 8 (11) (2017) 3855–3863.

[5] M. Rbaa, M. Galai, M. El Faydy, Y. Lakhrissi, M. Ebntouhami, A. Zarrouk, B. Lakhrissi, Synthesis and characterization of new quinoxaline derivatives of 8-hydroxyquinoline as corrosion inhibitors for mild steel in 1.0 M HCl medium, J. Mater. Environ. Sci. 9 (1) (2018) 172–188.

[6] J. Jiang, Y. Qiang, Z. Lei, J. Wang, Z. Qin, B. Xiang, Excellent corrosion inhibition performance of novel quinoline derivatives on mild steel in HCl media: experimental and computational investigations, J. Mol. Liq. 255 (2018) 53–63.

[7] V.S. Sastri, J.R. Perumareddi, Molecular orbital theoretical studies of some organic corrosion inhibitors, Corrosion 53 (8) (1997) 617–622.

[8] M. Rbaa, M. Galai, M.E.L. Faydy, Y. El Kacimi, M. Ebn Touhami, A. Zarrouk, B. Lakhrissi, Synthesis, inhibition effects and thermodynamic studies of novel substituted quinoline son the corrosion of mild steel in 1 M HCl solution, J. Mater. Environ. Sci. 8 (10) (2017) 3529–3549.

[9] M. Rbaa, M. Galai, M. El Faydy, Y. El Kacimi, M. Ebn Touhami, A. Zarrouk, B. Lakhrissi, Synthesis and characterization of new Benzimidazoles derivatives of 8-hydroxyquinoline as a corrosion inhibitor for mild steel in 1.0 M hydrochloric acid medium, Anal. Bioanal. Electrochemistry 9 (7) (2017) 904–928.

[10] M. El Faydy, M. Galai, M.E. Touhami, I.B. Obot, B. Lakhrissi, A. Zarrouk, Anticorrosion potential of some 5-amino-8-hydroxyquinolines derivatives on carbon steel in hydrochloric acid solution: gravimetric, electrochemical, surface morphological, UV–visible, DFT and Monte Carlo simulations, J. Mol. Liq. 248 (2017) 1014–1027.

[11] A. Yurt, A. Balaban, S.U. Kandemir, G. Bereket, B. Erk, Investigation on some Schiff bases as HCl corrosion inhibitors for carbon steel, Mater. Chem. Phys. 85 (2004) 420–426.

[12] M. Ehteshamzade, T. Shahrabi, M.G. Hosseini, Inhibition of copper corrosion by self-assembled films of new Schiff bases and their modification with alkanethiols in aqueous medium, Appl. Surf. Sci. 252 (2006) 2949–2959.

[13] M. Yadav, S. Kumar, R.P. Sinha, I. Bahadur, E.E. Ebenso, New pyrimidine derivatives as efficient organic inhibitors on mild steel corrosion in acidic medium: electrochemical, SEM, EDX, AFM and DFT studies, J. Mol. Liq. 211 (2015) 135–145.

[14] H. Tayebi, H. Bourazmi, B. Himmi, A. El Assyry, Y. Ramli, A. Zarrouk, A. Geunbour, B. Hammouti, Eno E. Ebenso, An electrochemical and theoretical evaluation of new quinoline derivative as a corrosion inhibitor for carbon steel in HCl solutions, Pharm. Lett. 6 (6) (2014) 20–34.

[15] G.J. Atwell, B.C. Baguley, W.A. Denny, Potential antitumor agents. 57. 2-Phenylquinoline-8-carboxamides as minimal DNA-intercalating antitumor agents with in vivo solid tumor activity, J. Med. Chem. 32 (1989) 396–401.

[16] M. Rbaa, M. Galai, Y. El Kacimi, M. Ouakki, R. Touir, B. Lakhrissi, M.E. Touhami, Adsorption properties and inhibition of carbon steel corrosion in a hydrochloric solution by 2-(4,5-diphenyl-4,5-dihydro-1h-imidazol-2-yl)-5-methoxyphenol, Port. Electrochim. Acta 35 (6) 323–338.

[17] D.K. Yadav, M.A. Quraishi, B. Maiti, Inhibition effect of some benzylidenes on mild steel in 1 M HCl: an experimental and theoretical correlation, Corros. Sci. 55 (2012) 254–266.

[18] A. Khadiri, R. Saddik, K. Bekkouche, A. Aouniti, B. Hammouti, N. Benchat, M. Bouachrine, R. Solmaz, Gravimetric, electrochemical and quantum chemical studies of some pyridazine derivatives as corrosion inhibitors for mild steel in 1 M HCl solution, J. Taiwan Inst. Chem. Eng. 58 (2016) 552–564.

[19] D.B. Hmamou, R. Salghi, A. Zarrouk, H. Zarrok, R. Touzani, B. Hammouti, A. El Assyry, Investigation of corrosion inhibition of carbon steel in 0.5 M H_2SO_4 by new bipyrazole derivative using experimental and theoretical approaches, J. Environ. Chem. Eng. 3 (3) (2015) 2031–2041.

[20] A. Popova, M. Christov, A. Vasilev, Inhibitive properties of quaternary ammonium bromides of N-containing heterocycles on acid mild steel corrosion. Part II: EIS results, Corros. Sci. 49 (2007) 3290–3302.

[21] M. Galai, M. Rbaa, Y. El Kacimi, M. Ouakki, N. Dkhirech, R. Touir, B. Lakhrissi, M. Ebn Touhami, Anti-corrosion properties of some Triphenylimidazole substituted compounds in corrosion inhibition of carbon steel in 1.0 M hydrochloric acid solution, Anal. Bioanal. Electrochemistry 9 (1) (2017) 80–101.

[22] P.M. Krishnegowda, V.T. Venkatesha, P.K.M. Krishnegowda, S.B. Shivayogiraju, Acalypha torta leaf extract as green corrosion inhibitor for mild steel in hydrochloric acid solution, Ind. Eng. Chem. Res. 52 (2013) 722–728.

[23] M.M. Fares, A.K. Maayta, M.M. Al-Qudah, Pectin as promising green corrosion inhibitor of aluminum in hydrochloric acid solution, Corros. Sci. 60 (2012) 112–117.

[24] A.K. Singh, S.K. Shukla, M.A. Quraishi, E.E. Ebenso, Investigation of adsorption characteristics of *N*,*N*′-[(methylimino) dimethylidyne] di-2,4-xylidine as corrosion inhibitor at mild steel/sulphuric acid interface, J. Taiwan Inst. Chem. Eng. 43 (2012) 463–472.

[25] S.K. Saha, A. Dutta, P. Ghosh, D. Sukul, P. Banerje, Novel Schiff-base molecules as efficient corrosion inhibitors for mild steel surface in 1 M HCl medium: experimental and theoretical approach, Phys. Chem. Chem. Phys. 18 (2016) 17898–17911.

[26] T. Laabaissi, M. Rbaa, M. Ourrak, H. Zarrok, M. El Faydy, B. Lakhrissi, H. Oudda, Adsorption properties and inhibition of carbon steel corrosion in hydrochloric acid solution by novel diazepine derivatives: experimental and theoretical studies, J. Mater. Environ. Sci. 9 (6) (2018) 1796–1808.

[27] H. Tayebi, H. Bourazmi, B. Himmi, A. El Assyry, Y. Ramli, A. Zarrouk, A. Geunbour, B. Hammouti, Combined electrochemical and quantum chemical study of new quinoxaline derivative as corrosion inhibitor for carbon steel in acidic media, Pharm. Lett. 6 (5) (2014) 220–234.

[28] D.K. Yadav, M.A. Quraishi, Application of some condensed uracils as corrosion inhibitors for mild steel: gravimetric, electrochemical, surface morphological, UV–visible, and theoretical investigations, Ind. Eng. Chem. Res. 51 (46) (2012) 14966–14979.

[29] P. Zhao, Q. Liang, Y. Li, Electrochemical, SEM/EDS and quantum chemical study of phthalocyanines as corrosion inhibitors for mild steel in 1 mol/l HCl, Appl. Surf. Sci. 252 (5) (2005) 1596–1607.

[30] K.R. Ansari, M.A. Quraishi, A. Singh, Corrosion inhibition of mild steel in hydrochloric acid by some pyridine derivatives: an experimental and quantum chemical study, J. Ind. Eng. Chem. 25 (2015) 89–98.

[31] M.A. Amin, K.F. Khaled, Q. Mohsen, H.A. Arida, A study of the inhibition of iron corrosion in HCl solutions by some amino acids, Corros. Sci. 52 (5) (2010) 1684–1695.

[32] M. Bhardwaj, R. Balasubramaniam, Uncoupled non-linear equations method for determining kinetic parameters in case of hydrogen evolution reaction following Volmer-Heyrovsky-Tafel mechanism and Volmer-Heyrovsky mechanism, Int. J. Hydrog. Energy 33 (9) (2008) 2178–2188.

[33] F. Bentiss, C. Jama, B. Mernari, H. El Attari, L. El Kadi, M. Lebrini, M. Lagrenée, Corrosion control of mild steel using 3,5-bis (4-methoxyphenyl)-4-amino-1,2,4-triazole in normal hydrochloric acid medium, Corros. Sci. 51 (8) (2009) 1628–1635.

[34] M. Behpour, S.M. Ghoreishi, N. Mohammadi, N. Soltani, M. Salavati-Niasari, Investigation of some Schiff base compounds containing disulfide bond as HCl corrosion inhibitors for mild steel, Corros. Sci. 52 (2010) 4046–4057.

[35] D.K. Yadav, B. Maiti, M.A. Quraishi, Electrochemical and quantum chemical studies of 3,4-dihydropyrimidin-2 (1H)-ones as corrosion inhibitors for mild steel in hydrochloric acid solution, Corros. Sci. 52 (2010) 3586–3598.

[36] N. Dkhireche, M. Galai, Y. El Kacimi, M. Rbaa, M. Ouakki, B. Lakhrissi, M.E. Touhami, New quinoline derivatives as sulfuric acid inhibitor's for mild steel, Anal. Bioanal. Electrochem. 10 (1) (2018) 111–135.

[37] I.B. Obot, N.O. Obi-Egbedi, S.A. Umoren, Adsorption characteristics and corrosion inhibitive properties of clotrimazole for aluminium corrosion in hydrochloric acid, Int. J. Electrochem. Sci. 4 (2009) 863–877.

[38] M. Ouakki, M. Rbaa, M. Galai, B. Lakhrissi, E.H. Rifi, M. Cherkaoui, Experimental and quantum chemical investigation of imidazole derivatives as corrosion inhibitors on mild steel in 1.0 M hydrochloric acid, journal of bio-and tribo, Corrosion 4 (3) (2018) 1–14.
[39] H. Keles, M. Keles, I. Dehri, O. Serindag, The inhibitive effect of 6-amino-m-cresol and its Schiff base on the corrosion of mild steel in 0.5 M HCl medium, Mater. Chem. Phys. 112 (2008) 173–179.
[40] S.Q. Hu, J.Q. Hu, C.C. Fan, X.L. Jia, J. Zhang, W.Y. Guo, Theoretical and experimental study of corrosion inhibition performance of new imidazoline corrosion inhibitors, Acta Chim. Sin. 68 (2010) 2051–2058.
[41] D. Daoud, T. Douadi, H. Hamani, S. Chafaa, M. Al-Noaimi, Corrosion inhibition of mild steel by two new S-heterocyclic compounds in 1 M HCl: experimental and computational study, Corros. Sci. 94 (2015) 21–37.
[42] L. Guo, S. Zhu, S. Zhang, Experimental and theoretical studies of benzalkonium chloride as an inhibitor for carbon steel corrosion in sulfuric acid, J. Ind. Eng. Chem. 24 (2015) 174–180.
[43] Y. Zhou, S. Xu, L. Guo, S. Zhang, H. Lu, Y. Gong, F. Gao, Evaluating two new Schiff bases synthesized on the inhibition of corrosion of copper in NaCl solutions, RSC Adv. 5 (2015) 14804–14813.
[44] Y. Kharbach, F.Z. Qachchachi, A. Haoudi, M. Tourabi, A. Zarrouk, C. Jama, L.O. Olasunkanmi, E.E. Ebenso, F. Bentiss, Anticorrosion performance of three newly synthesized isatin derivatives on carbon steel in hydrochloric acid pickling environment: electrochemical, surface and theoretical studies, J. Mol. Liq. 246 (2017) 302–316.